NACA TN 3762

NATIONAL ADVISORY COMMITTEE FOR AERONAUTICS

TECHNICAL NOTE 3762

DRAG COEFFICIENTS FOR DROPLETS AND SOLID SPHERES IN CLOUDS ACCELERATING IN AIRSTREAMS

By Robert D. Ingebo

Lewis Flight Propulsion Laboratory
Cleveland, Ohio

Washington

September 1956

NATIONAL ADVISORY COMMITTEE FOR AERONAUTICS

TECHNICAL NOTE 3762

DRAG COEFFICIENTS FOR DROPLETS AND SOLID SPHERES IN CLOUDS ACCELERATING IN AIRSTREAMS

By Robert D. Ingebo

SUMMARY

Clouds of liquid and solid spheres accelerating in airstreams were studied over a range of airstream pressure, temperature, and velocity conditions. Diameter and velocity data for individual droplets and solid spheres in the clouds were obtained with a high-speed camera developed at the NACA Lewis laboratory. From these data, linear accelerations of spheres (20 to 120 microns in diam.) were determined, and instantaneous drag coefficients for unsteady momentum transfer were calculated. The drag coefficients C_D for droplets (isooctane, water, and trichloroethylene) and solid spheres (magnesium and calcium silicide) were found to correlate Reynolds number Re as given by the empirical expression $C_D = 27/Re^{0.84}$, for $6 < Re < 400$. When acceleration rates were low, the unsteady-state drag coefficients were in agreement with steady-state values from previous investigations. From this expression for drag coefficient, an equation relating distance and time was derived for calculating trajectories of solid spheres. In the case of droplets, a graphical method was used to relate droplet diameter to distance when evaporation rates were high. When evaporation rates were low, solid-sphere trajectory equations were found applicable.

INTRODUCTION

The steps preceding burning of liquid fuel injected into a combustor, that is, atomization, acceleration, and vaporization, are important in the design, operation, and performance of jet engines (ref. 1). The droplets formed by atomization simultaneously accelerate and evaporate giving combustible fuel-air mixtures. In the vaporization process, the driving potential (temperature difference) may be assumed constant when air temperature is constant and the droplet surface temperature is approximately equal to the wet-bulb temperature. Thus, steady-state heat transfer may be assumed, and there are considerable data in the literature on the vaporization rate of droplets for this case (refs. 2 and 3).

During acceleration, the transfer of momentum to spheres may be considered a case of unsteady-state momentum transfer since the difference between airstream and sphere velocity varies with time. Considerable data are available for steady-state momentum transfer where solid spheres are suspended in airstreams (ref. 4), but very little data for unsteady transfer of momentum. Because of the lack of such data, it is often assumed that steady-state drag-coefficient data may be directly applied to accelerating spheres. This would mean frictional drag due to viscous shear and form drag due to surface pressure variations would be the same in both cases. In reference 5, a theoretical treatment indicates that the effect of acceleration on the drag coefficient is minor when the ratio of the air to sphere density is low. However, data on free-falling spheres (refs. 6 and 7) give some disagreement with steady-state drag coefficients even though terminal velocities were reached and nearly steady-state conditions existed. Thus, it is questionable whether or not steady momentum transfer rates are directly applicable to unsteady momentum transfer.

The work of reference 8 was a preliminary investigation of accelerating clouds of isooctane droplets. However, momentum transfer rates could not be determined accurately, since the liquid was atomized over a relatively large penetration distance, and the initial point of droplet acceleration could not be determined. The initial point of acceleration was established in the present study by atomizing the liquid on a screen. Acceleration data were obtained for solid spheres, nonevaporating droplets, and evaporating droplets ranging in diameter from 20 to 120 microns. Three liquids (isooctane, water, and trichloroethylene) and two solids (magnesium and calcium silicide) were used in the present investigation. Water droplets accelerating in airstreams of 100-percent relative humidity were used for the nonevaporating case. Sphere diameter and velocity data were obtained with the high-speed camera described in reference 8. Wet-bulb data were obtained for trichloroethylene for heat-transfer calculations. Air temperatures of 40° to 700° F, air static pressures of 12.7 to 49 inches of mercury, and air velocities of 100 to 180 feet per second were used; and sphere densities ranged from 0.69 to 2.5 grams per cubic centimeter. From these data, it was possible to calculate instantaneous drag coefficients for unsteady momentum transfer from airstreams to accelerating spheres and to derive equations for calculating sphere trajectories.

SYMBOLS

The following symbols are used in this report:

A	projected area of sphere, sq cm
a	acceleration of sphere, cm/sec^2
C_D	instantaneous drag coefficient, $ma/\rho_a A(\Delta U)^2$

C'_D	drag coefficient based on equation $(ma + \Delta U\, dm/dt) = \frac{1}{2} \rho_a A(\Delta U)\, C'_D$
$\bar{c}$	root-mean-square velocity of air molecules, cm/sec
$D_{g,M}$	molecular mass diffusivity, g/(cm)(sec)
$\mathscr{D}$	sphere diameter, cm
g	acceleration due to gravity, 980 cm/sec^2
H_v	latent heat of vaporization, g-cal/g
h	heat-transfer coefficient, g-cal/(sec)(sq cm)(^oC)
k	thermal conductivity, g-cal/(sec)(sq cm)(^oC)/(cm)
l	mean free path of air molecules, cm
m	mass of liquid, g
dm/dt	vaporization rate, g/sec
Nu	heat-transfer Nusselt number, $h\mathscr{D}/k$
n	number of droplets in given size range
p_a	airstream static pressure, in. Hg abs
Re	Reynolds number based on sphere diameter and average film temperature, $\mathscr{D}\Delta U\rho_a/\mu_a$
Sc	Schmidt number, $\mu_a/D_{g,M}$
T	temperature, ^oC
ΔT	difference between air temperature and surface temperature of droplet, $T_a - T_d$, ^oC
t	time, sec
U	velocity, ft/sec
ΔU	relative velocity of air with respect to droplet, cm/sec

x distance downstream from injector orifice, cm

η_v portion of total spray that has evaporated, percent

μ fluid viscosity, poises

ρ fluid density, g/cu cm

Subscripts:

a air

av average

d droplet

i initial condition

l liquid

s sphere

v vapor

APPARATUS AND PROCEDURE

The velocity of microscopic liquid droplets and solid spheres accelerating in airstreams was determined experimentally with the apparatus shown in figures 1 and 2. Air at $82^\circ \pm 3^\circ$ F and 16 $\pm$1 percent relative humidity, supplied from the central laboratory system, was metered with a variable-area orifice and exhausted to the altitude exhaust system. Velocity profiles in the 8-inch-inside-diameter test section showed velocity variations of less than 2 percent for points up to within 1 inch of the wall. The air velocity and pressure were controlled by upstream and downstream valves. An air temperature of $700^\circ \pm 5^\circ$ F in the test section was obtained by burning JP-4 fuel in the turbojet-engine combustor shown in figure 1.

Isooctane (2,2,4-trimethylpentane), water, and trichloroethylene, all of which met A.S.T.M. specifications, were used in the spray tests. The liquid was injected from a nozzle that spread a flat sheet of liquid across a 50-by-40-mesh, 0.0095-inch-diameter, stainless-steel wire screen placed across the duct 1/4 inch downstream of the nozzle. A suspension of calcium silicide spheres in air was formed by the electric motor and blower shown in figure 2. After the screen was removed from the test section, the dust suspension was fed slowly into the test section through

an open-end 1/4-inch-diameter tube. In the case of magnesium, a dust suspension was formed by blowing nitrogen through a loose bed of solids. Photomicrographs of samples of the magnesium and calcium silicide used in this study are shown in figure 3.

Droplet size and velocity data were obtained for spheres ranging from 20 to 120 microns in diameter by photographing clouds of spheres at several distances downstream of the injector. Photomicrographs taken at the centerline of the clouds and at radial points in cloud cross sections showed no apparent effect of the radial position of the droplets on the relation between droplet size and velocity. A diagram of the optics of the high-speed camera used in this study is shown in figure 2, and further description of the camera is given in reference 8.

The camera utilized a rotating mirror which tracked the spheres, and sequences of photomicrographs such as those shown in figure 4 were obtained for ranges of mirror speeds. When mirror speeds were too fast or too slow, droplet images were found to be smeared on the film and diameters could not be determined. However, at intermediate mirror speeds, droplet images were stopped on the film and their velocities determined from the corresponding mirror speeds. Measurements of droplet or solid-sphere diameters were made from the photomicrographs with an accuracy of ± 3 microns. Velocities were calculated from mirror speeds with an accuracy of ± 5 feet per second. Thus, droplet size and velocity data were obtained for the conditions shown in table I. Wet-bulb data for trichloroethylene were obtained experimentally using the technique described in references 2 and 3. From these data it was possible to calculate drag coefficients for evaporating droplets, nonevaporating droplets, and solid spheres.

RESULTS AND DISCUSSION

Results of this investigation are for unsteady momentum transfer from airstreams to clouds of (1) solid spheres and nonevaporating droplets and (2) evaporating droplets. Drag-coefficient equations are presented, and data for accelerating spheres in clouds are discussed in relation to data for fixed spheres and free-falling drops.

Momentum Transfer to Solid Spheres and Nonevaporating Droplets

Equating the force accelerating a sphere with the aerodynamic pressure force of an airstream gives the following force balance:

$$ma = \frac{1}{2} \rho_a A (\Delta U)^2 C_D \qquad (1)$$

If this equation is assumed valid at any instant (in the case of unsteady momentum transfer), then the instantaneous drag coefficient may be given by the following expression:

$$C_D = \frac{4}{3} \frac{\rho_s}{\rho_a} \frac{\mathscr{D}a}{(\Delta U)^2} \qquad (2)$$

where $a = \frac{1}{2} d(U_s^2)/dx$. In this investigation, the linear acceleration a was determined. Actually, a sphere in free flight may have angular acceleration or "spin." Velocity gradients present in airstreams within a cloud of spheres could produce rotary motion similar to that observed for a ball in an air jet. Since angular acceleration could not be measured with the camera, drag-coefficient calculations were based on linear acceleration.

In equation (1), $\Delta U = U_a - U_s$ where U_s was determined directly from the camera mirror speed. However, the velocity of airstreams within the clouds of spheres could not be measured directly. Photomicrographs were taken at radial positions across the entire cross sections of the clouds of spheres, and spheres of a given size had approximately the same velocity regardless of their radial position in the cloud cross section. Also, varying injection rates from 10 to 100 pounds per hour showed negligible effect on sphere velocity and diameter data. Thus, U_a was assumed approximately constant across all cloud cross sections and approximately equal to free-stream velocity in calculating drag coefficients.

Correlation of Drag Coefficient with Reynolds Number

From the droplet sphere diameter and velocity data presented in figures 5 to 10, linear acceleration was calculated by plotting experimental values of U_s^2 against x and determining slopes from the curves. Sample plots are shown in figure 11. Using equation (2) and slopes from plots similar to figure 11, drag coefficients were calculated and plotted against Reynolds numbers ($6 < Re < 400$) as shown in figure 12. Stokes' law and drag-coefficient data for fixed solid spheres (ref. 4) and free-falling water droplets (ref. 6) are included for comparison. From this plot, the following empirical expression was obtained for the instantaneous unsteady-state drag coefficient based on linear acceleration:

$$C_D = 27/Re^{0.84} \qquad (3)$$

which may be substituted into equation (1) to give

$$ma = \frac{1}{2} \rho_a A(\Delta U)^2 \, 27/Re^{0.84} \qquad (4)$$

Thus, a correlation of drag coefficient with Reynolds number was obtained for magnesium and calcium silicide spheres accelerating in airstreams and nonevaporating water droplets accelerating in airstreams of 100-percent relative humidity.

Figure 12 shows that instantaneous unsteady-state drag coefficients fall between Stokes' law and steady-state values. A fundamental explanation of this disagreement with steady-state values cannot be obtained directly from the camera data. Thus, further knowledge is required concerning unsteady transfer of momentum from airstreams to clouds of accelerating spheres to clarify this point. However, some possible explanations may be considered as follows:

(1) The instantaneous flow field around an accelerating sphere (particularly in the wake) may be considerably more streamlined at high Reynolds numbers than is flow around the single fixed sphere. A theoretical treatment of the effect of accelerated motion on displacement of air in the wake of a sphere is given in reference 9 that indicates flow lines are different with acceleration.

(2) The velocity of airstreams within clouds of accelerating spheres could not be measured directly and may be considerably less than free-stream velocity especially in the region near the injector where the droplets gain momentum at a very fast rate. As the cloud moved downstream and droplet acceleration decreased, airstream velocity in the cloud could be increased by momentum transferred from the surrounding air into the cloud of droplets. Under these conditions, measurements would show reduced total air pressure within the cloud. At present, no instrument is available for use in making these measurements.

(3) Because of small-scale velocity gradients in airstreams in clouds of accelerating microscopic spheres, angular as well as linear acceleration may result from the momentum transfer process. Thus, a low drag coefficient would be calculated on the basis of linear acceleration alone. Calculations show that this phenomenon could account for only a small part of the observed differences between the unsteady-state and steady-state drag coefficients.

(4) In this study, spheres of 20 to 120 microns in diameter were used, whereas in the case of free-falling drops and fixed solid spheres (refs. 4, 6, and 7) the diameters were of the order of 1000 microns.

(5) Accelerations of the order of 60,000 feet per second squared were calculated in this investigation compared to a maximum acceleration of 32.2 feet per second squared for free-falling droplets (refs. 6 and 7).

All the unsteady-state drag-coefficient data of figure 12 fall on a common curve that agrees with steady-state values at low Reynolds numbers but differ considerably at high Reynolds numbers from the steady-state curve. This leads to the speculation that the unsteady-state curve may represent limiting values that are reached only with the very small spheres and very high acceleration rates investigated herein. For larger spheres that would give lower acceleration rates for the high Reynolds numbers, it is possible that data points would fall between the unsteady-state and the steady-state curves of figure 12.

Derivation of Trajectory Equations

In order to obtain a more useful expression for calculating trajectories of spheres, dU_s/dt may be substituted for acceleration a in equation (4). Integrating from $\Delta U = U_a$ to $\Delta U = \Delta U$ and from $t = 0$ to $t = t$ gives

$$t = 0.31 \frac{\rho_l \mathscr{D}^2}{\mu_a Re_i^{0.16}} \left[\left(\frac{U_a}{\Delta U} \right)^{0.16} - 1 \right] \tag{5}$$

where Re_i is the initial Reynolds number $\mathscr{D} U_a \rho_a / \mu_a$. Thus, a relation between time and velocity difference is obtained. A relation between distance and velocity difference may be found by substituting $U_s dU_s/dx$ for acceleration a in equation (4) and integrating from $\Delta U = U_a$ to $\Delta U = \Delta U$ and from $t = 0$ to $t = t$ to give

$$x = 0.058 \frac{\rho_s}{\rho_a} \mathscr{D} Re_i^{0.84} \left[\left(\frac{\Delta U}{U_a} \right)^{0.84} + 5.25 \left(\frac{U_a}{\Delta U} \right)^{0.16} - 6.25 \right] \tag{6}$$

Combining equations (5) and (6) gives the following relation between distance x and time t:

$$x = 0.059 \frac{\rho_l}{\rho_a} \mathscr{D} Re_i^{0.84} \left[\left(1 + \frac{3.23 \rho_a}{\rho_l} \frac{t U_a}{\mathscr{D} Re_i^{0.84}} \right)^{-5.25} + 5.25 \left(1 + \frac{3.23 \rho_a}{\rho_l} \frac{t U_a}{\mathscr{D} Re_i^{0.84}} \right) - 6.25 \right] \tag{7}$$

This equation may be readily applied to the calculation of sphere trajectories for conditions similar to those used in this investigation.

Momentum Transfer to Evaporating Droplets

In reference 7 the following force balance is used to estimate drag coefficients for isooctane droplets:

$$ma + \Delta U \frac{dm}{dt} = \frac{1}{2} \rho_a A(\Delta U)^2 C_D' \qquad (8)$$

For this investigation, the unsteady-state drag coefficient is redefined so that at any instant $ma = 1/2\ \rho_a A(\Delta U)^2 C_D$. This equation is the same as equation (1) for solid spheres and assumes that vapor leaving the droplet surface has a negligible effect on the drag coefficient. Thus, the instantaneous drag coefficients for liquid and solid spheres should agree for corresponding Reynolds numbers if equation (1) holds for both liquid and solid spheres.

Correlation of Droplet Drag Coefficient with Reynolds Number

Drag coefficients of evaporating droplets were calculated from droplet diameter and velocity data given in figures 8 to 10 in the following manner: The change in diameter $d\mathscr{D}$ was calculated for the distance increments of 2, 3, and 4 inches using the vaporization-rate equation:

$$\frac{d\mathscr{D}}{dx} = \frac{2k_a \Delta T}{\rho_l H_v} \left(\frac{Nu}{\mathscr{D} U_d} \right)_{av} \qquad (9)$$

where

$$Nu = 2 + 2.58 \times 10^6 \left(ReScg_l / \bar{c}^2 \right)^{0.6} \left(k_a / k_v \right)^{0.5}$$

as given in reference 1. Calculations for liquids in 82° F airstreams showed $d\mathscr{D}$ to be small for correspondingly large changes in droplet velocity. Thus, acceleration was determined directly from curves shown in figure 11. Drag coefficients calculated from equation (1) are plotted against Reynolds number in figure 12. This plot shows that the correlation of drag coefficient with Reynolds number is approximately the same for slowly evaporating drops, nonevaporating drops, and solid spheres. Thus, defining C_D such that $ma = 1/2\ \rho_a A(\Delta U)^2 C_D$ appears reasonable for these tests.

For the case of trichloroethylene droplets evaporating in 700° F airstreams, values of $d\mathscr{D}$ were relatively large. Figure 13 shows U_d^2 plotted against x for two initial droplet sizes and subsequent instantaneous droplet diameters calculated from equation (9). Comparison of this figure with figure 11 shows that rapidly evaporating droplets have an apparent increasing rate of acceleration with distance, whereas slowly evaporating droplets have a continuously decreasing rate. However, the plot of instantaneous drag coefficient against Reynolds number (fig. 12) shows the same correlation of drag coefficient with Reynolds number for rapidly evaporating droplets, slowly evaporating droplets, nonevaporating droplets, and solid spheres. Thus, defining C_D such that $ma = \frac{1}{2}\rho_a A(\Delta U)^2 C_D$ gave good agreement even at relatively high vaporization rates, and the acceleration of vapor from the droplets appeared to have negligible effect on their drag coefficients.

Drag coefficients for isooctane sprays calculated in reference 8 do not agree with those determined in this investigation for two reasons. First, contrastream injection was used in reference 8, which gave penetration as well as atomization of the liquid, and droplet velocity appeared to be independent of droplet diameter at the camera station. This could be explained by large drops penetrating relatively large distances upstream of the injector and therefore having time to accelerate to approximately the same velocity at the camera station as small droplets that penetrated small distances upstream of the injector. Thus, penetration of the injected liquid masked the relation between droplet diameter and velocity in reference 8. The second reason for disagreement with reference 8 is that data on accelerating microscopic solid spheres and nonevaporating droplets were not available, and the effect of vaporization rate on the drag coefficient could not be directly established in reference 8. However, by applying equations derived in the present investigation to drop-size-distribution data given in reference 8, as shown in the appendix, good agreement is found between the calculated and experimental weight percent of the spray evaporated. Thus, the plots of drag coefficient against Reynolds number given in reference 8 should be disregarded, since results from the investigation herein show that droplet velocity data cannot be directly extrapolated back to the injector in the case of contrastream injection.

Graphical Integration Method for Calculating Droplet Trajectory

For the initial condition of droplet acceleration, assume $\Delta U = U_a$, and equation (4) may be rewritten as

$$ma_i = \frac{1}{2}\rho_a A U_a^2 \, 27/Re_i^{0.84} \qquad (11)$$

If equation (4) is divided by equation (11), we find that

$$\frac{a}{a_i} = \left(\frac{\Delta U}{U_a}\right)^{1.16}\left(\frac{\mathscr{D}_i}{\mathscr{D}}\right)^{1.84} \tag{12}$$

This expression gives the relation between acceleration, velocity difference, and diameter at any instant as based on the initial values of these variables.

In order to obtain a relation between droplet diameter and velocity difference, equations (4) and (9) may be combined to give the resulting equation independent of time:

$$\frac{d\mathscr{D}}{dU_s} = 0.099\,\frac{\mathscr{D}}{\Delta U}\left(\frac{k_a \Delta T}{\mu_a H_v}\right)\frac{Nu}{Re^{0.16}} \tag{13}$$

Thus, a plot of $\mathscr{D}$ against U_s may be made as shown in figure 14. From this, a relation between $\mathscr{D}$ and ΔU is established. Equation (12) may be rewritten as

$$\frac{dU_s^2}{dx} = 2\,a_i\left(\frac{\Delta U}{U_a}\right)^{1.16}\left(\frac{\mathscr{D}_i}{\mathscr{D}}\right)^{1.84} \tag{14}$$

A plot of U_s^2 against x may be constructed from equation (14) by using values of $\mathscr{D}$ and ΔU obtained from the plot of equation (13). Thus, graphical integration of equations (13) and (14) gives the droplet diameter and velocity at any distance x. The method of applying these equations to spray evaporation (ref. 8) is given in the appendix.

SUMMARY OF RESULTS

An analysis of data for unsteady momentum transfer from airstreams to clouds of solid spheres, nonevaporating droplets, and evaporating droplets gave the following correlation of drag coefficient with Reynolds number:

$$C_D = 27/Re^{0.84}$$

for a Reynolds number range of 6 to 400 and a sphere diameter range of 20 to 120 microns. Rapid variations in acceleration and velocity difference with time gave instantaneous drag coefficients between Stokes'

law and steady-state values. Near the end of the acceleration period, when acceleration and velocity differences were low, unsteady-state drag coefficients agreed with steady-state values.

Lewis Flight Propulsion Laboratory
National Advisory Committee for Aeronautics
Cleveland, Ohio, May 10, 1956

APPENDIX - APPLICATION OF DRAG-COEFFICIENT EQUATIONS TO SPRAY EVAPORATION

The drag-coefficient expression derived in this investigation and single-droplet vaporization-rate equations may be applied to sprays when the droplet size distribution is known. The following stepwise procedure is recommended:

(1) Take a size range (e.g., 0 to 10 microns) and, using the average diameter (5 microns), construct a plot of $\mathscr{D}$ against U_s from equation (13). Using equation (14), construct a plot of U_s^2 against x. Repeat this procedure for the remaining size range.

(2) Calculate $\sum n\mathscr{D}_i^3$ where $\mathscr{D}_i$ is the average initial drop size (5 microns for the first size range) for the given number of droplets n.

(3) At the desired distance x, obtain values of $\mathscr{D}$ from the plots of equations (13) and (14). Calculate $\sum n\mathscr{D}^3$ where n is the same number as that of the corresponding initial size range.

(4) Calculate the percentage evaporated η_v from the following equation:

$$\eta_v = 100\frac{\sum n\mathscr{D}_i^3 - \sum n\mathscr{D}^3}{n\mathscr{D}_i^3}$$

Application of this method to droplet-size-distribution data given in reference 8 gave the following results:

U_a, ft/sec	Experimental $\sum n\mathscr{D}_i^3$, cu cm (x = 5.5 in.)	Calculated $\sum n\mathscr{D}^3$, cu cm (x = 14 in.)	Percent evaporated (from x = 5.5 in. to x = 14 in.)	
			Calculated	Experimental
140	1731×10^{-7}	1486×10^{-7}	14.1	14.4
180	1051×10^{-7}	837×10^{-7}	16.9	15.1

Thus, the graphical-integration method gave results in good agreement with values obtained from direct integration of droplet-size-distribution data for isooctane sprays.

REFERENCES

1. Clarke, J. S.: The Relation of Specific Heat Release to Pressure Drop in Aero-Gas-Turbine Combustion Chambers. Sec. 5: Gas Turbines. The Inst. Mech. Eng. (London), and A.S.M.E. Joint Conf. on Combustion, 1955, pp. 24-31.

2. Ingebo, Robert D.: Vaporization Rates and Heat-Transfer Coefficients for Pure Liquid Drops. NACA TN 2368, 1951.

3. Ingebo, Robert D.: Study of Pressure Effects on Vaporization Rate of Drops in Gas Streams. NACA TN 2850, 1953.

4. Perry, John H., ed.: Chemical Engineers' Handbook. Third ed., McGraw-Hill Book Co., Inc., 1950, p. 1018.

5. Hughes, R. R., and Gilliland, E. R.: The Mechanics of Drops. Chem. Eng. Prog., vol. 48, no. 10, Oct. 1952, pp. 497-504.

6. Laws, J. Otis: Measurements of the Fall-Velocity of Water-Drops and Raindrops. Trans. Am. Geophys. Union, vol. 22, pt. 3, 1941, pp. 709-721; discussion, p. 721.

7. Lunnon, R. G.: Fluid Resistance to Moving Spheres. Proc. Roy. Soc. (London), ser. A, vol. 110, no. A 754, Feb. 1, 1926, pp. 302-326.

8. Ingebo, Robert D.: Vaporization Rates and Drag Coefficients for Isooctane Sprays in Turbulent Air Streams. NACA TN 3265, 1954.

9. Prandtl, L., and Tietjens, O. G.: Applied Hydro- and Aeromechanics. McGraw-Hill Book Co., Inc., 1934, p. 107.

TABLE I. - EXPERIMENTAL CONDITIONS

Spheres		Gas conditions			
Material	Density, g/cu cm	Gas	U_a, ft/sec	p_a, in. Hg	T_a, °F
Calcium silicide	2.50	Air	100	41.2	82
	2.50	Air	140	29.3	82
Magnesium	1.74	Air	180	29.3	82
Trichloro-ethylene	1.46	Air	100	41.2	82
	↓	↓	140	29.3	82
			180	29.3	82
			180	49.0	700
Water	1.00	Air	100	41.2	82
	↓	↓	140	29.3	82
			180	29.3	82
			180	12.7	82
		Air saturated with water vapor	180	12.7	40
Isooctane	0.69	Air	100	41.2	82
	↓	↓	140	29.3	82
			180	29.3	82

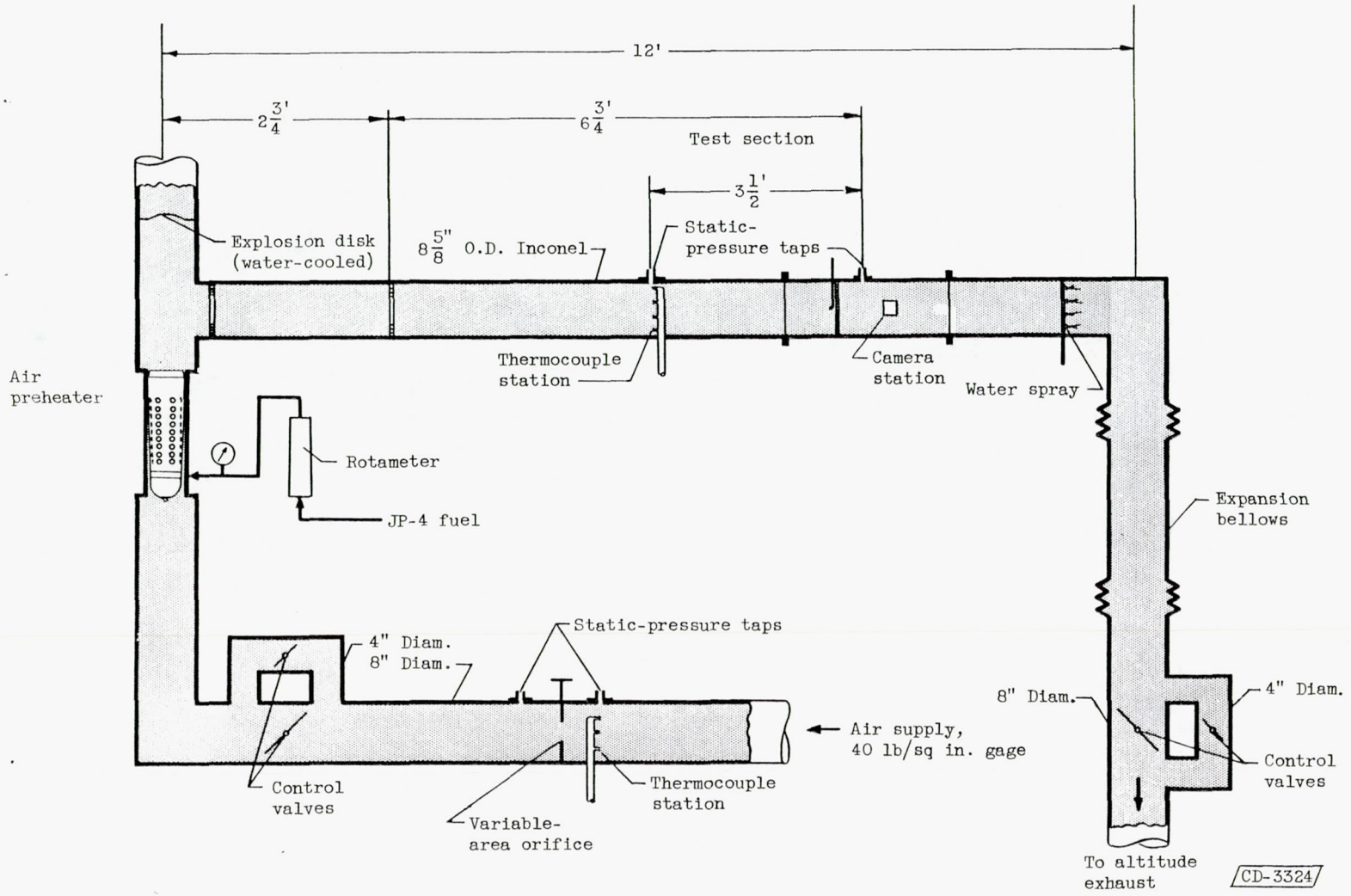

Figure 1. - Schematic drawing of test installation.

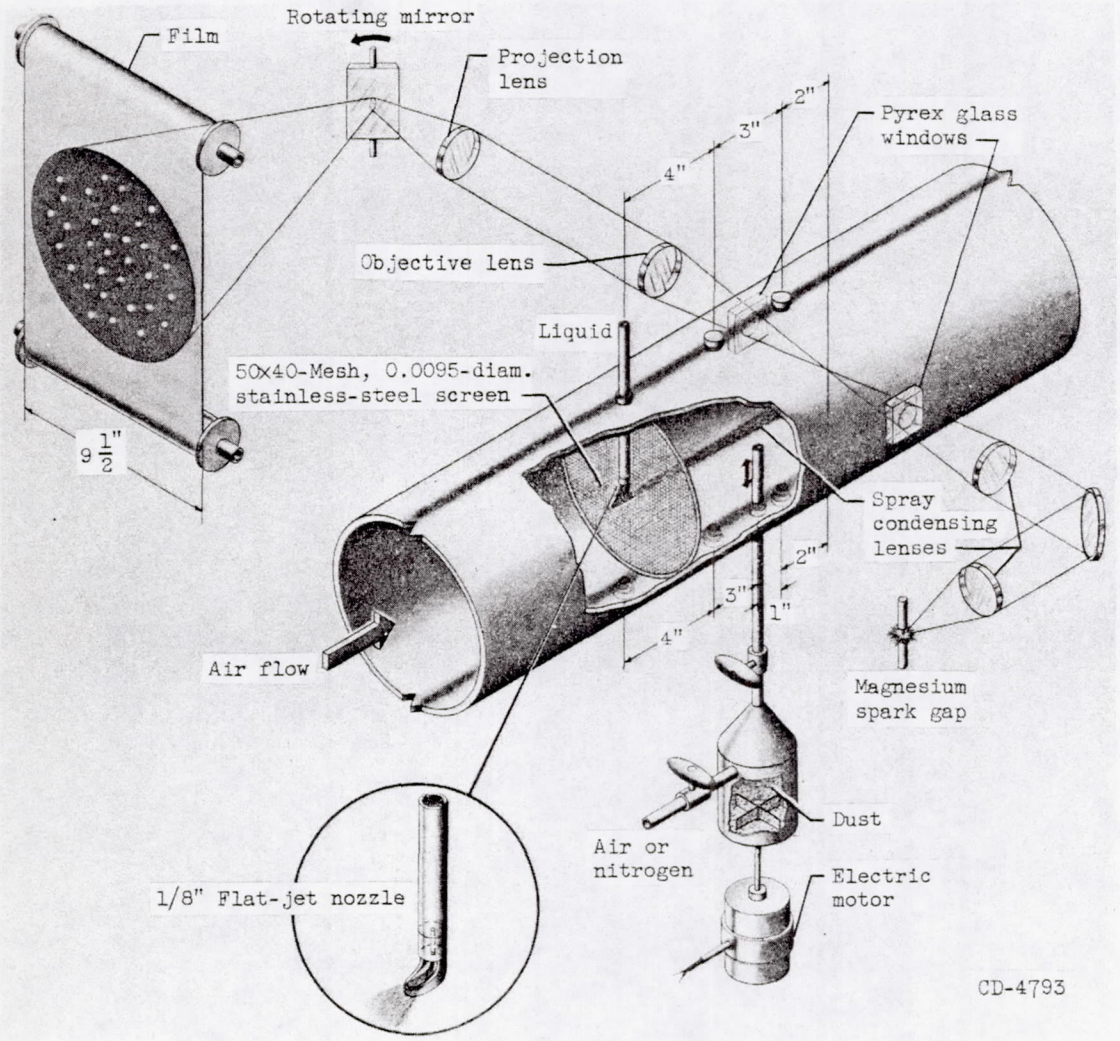

Figure 2. - Diagram of test-section equipment.

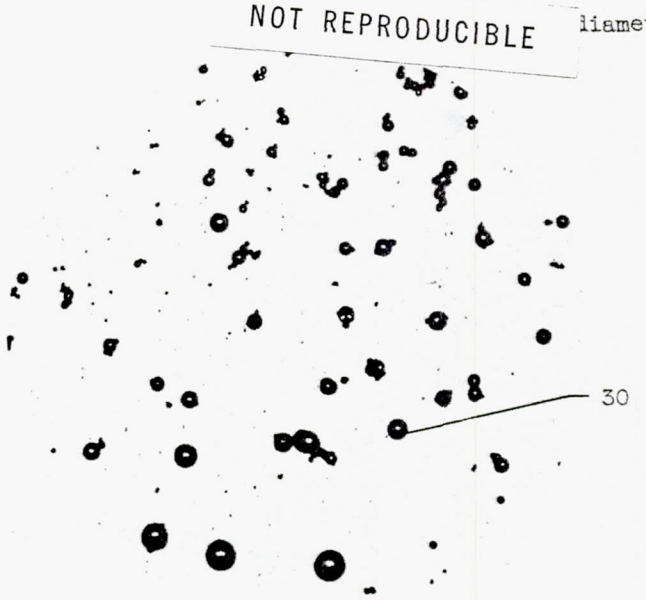

(a) Magnesium.

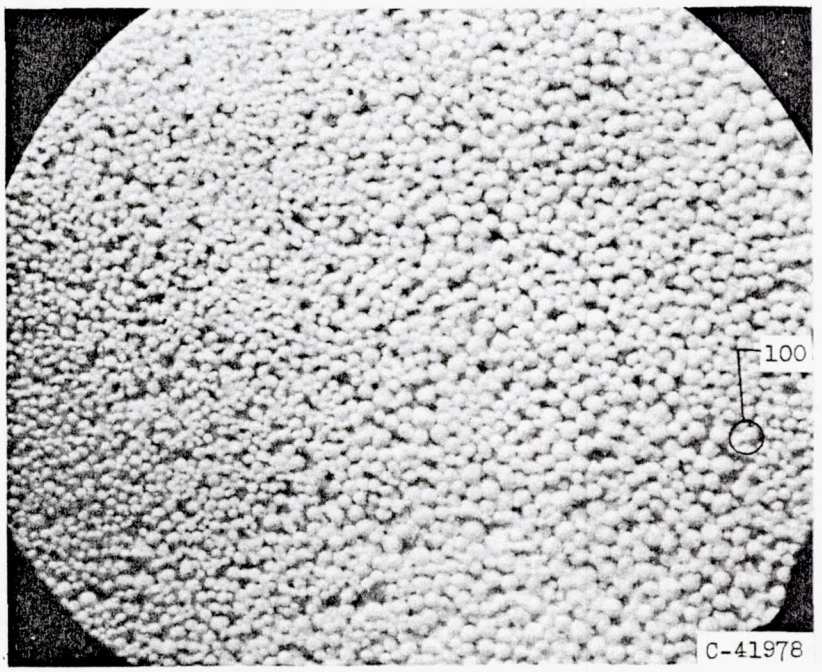

(b) Calcium silicide.

Figure 3. - Photomicrographs of samples of solid spheres on glass slides.

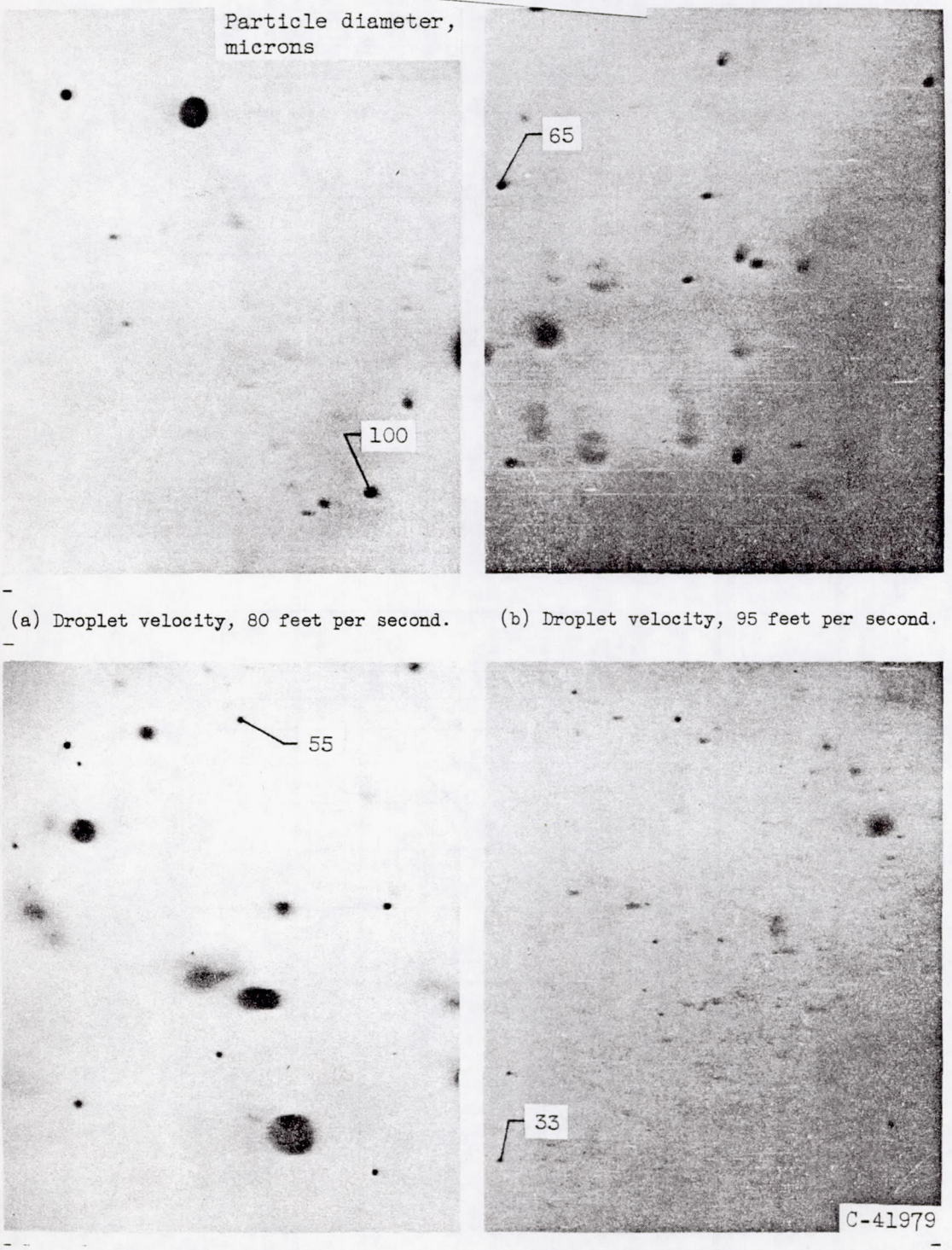

(a) Droplet velocity, 80 feet per second.

(b) Droplet velocity, 95 feet per second.

(c) Droplet velocity, 105 feet per second.

(d) Droplet velocity, 120 feet per second

Figure 4. - Sequence of water-droplet photomicrographs for range of mirror speeds. Distance downstream from wire screen, 5 inches; airstream velocity, 140 feet per second; air static pressure, 29.3 inches of mercury absolute; air temperature, 82° F.

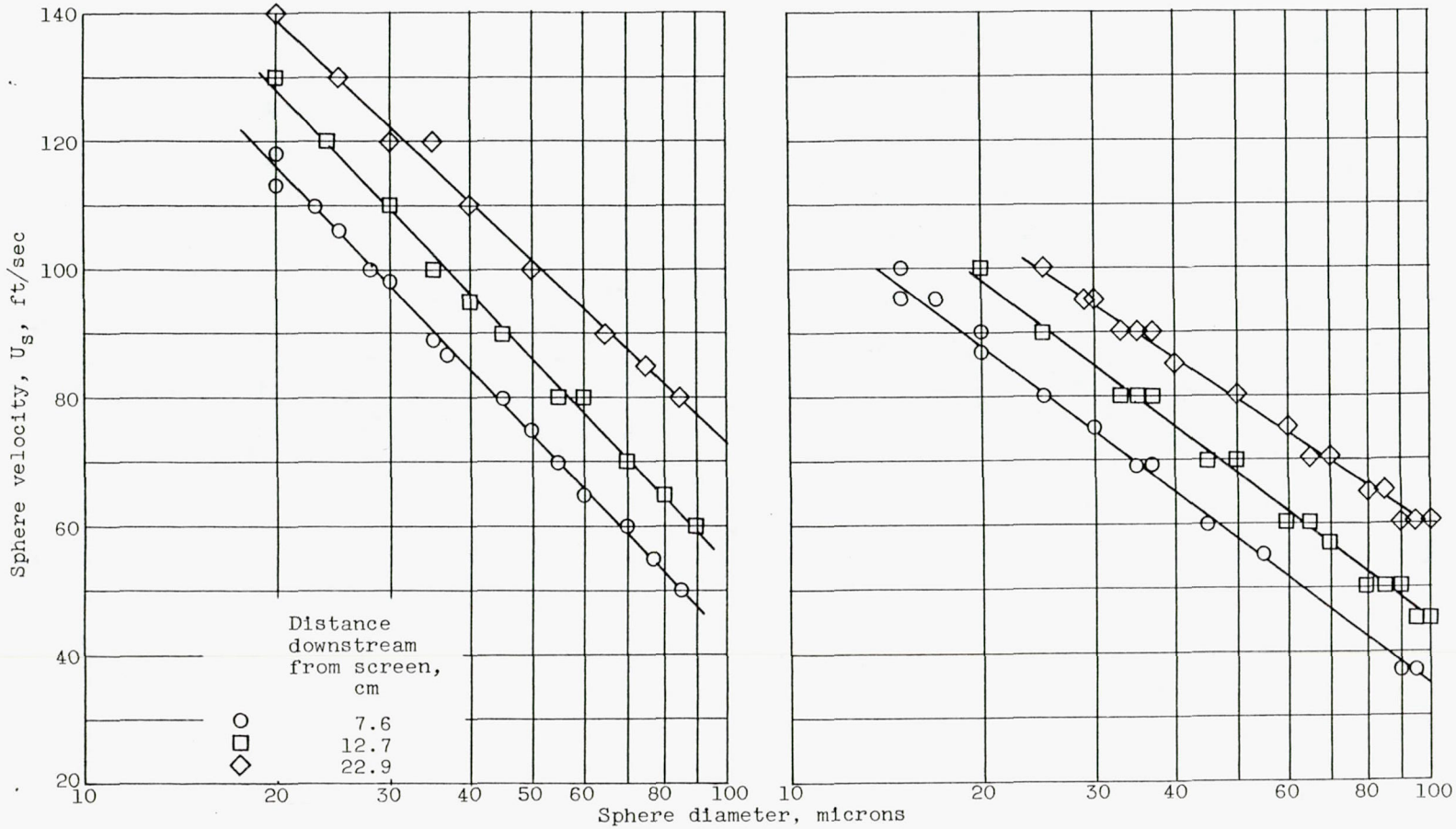

(a) Airstream velocity, 140 feet per second; air static pressure, 29.3 inches of mercury absolute.

(b) Airstream velocity, 100 feet per second; air static pressure, 41.2 inches of mercury absolute.

Figure 5. - Velocity and diameter data for calcium silicide spheres. Air temperature, 82° F.

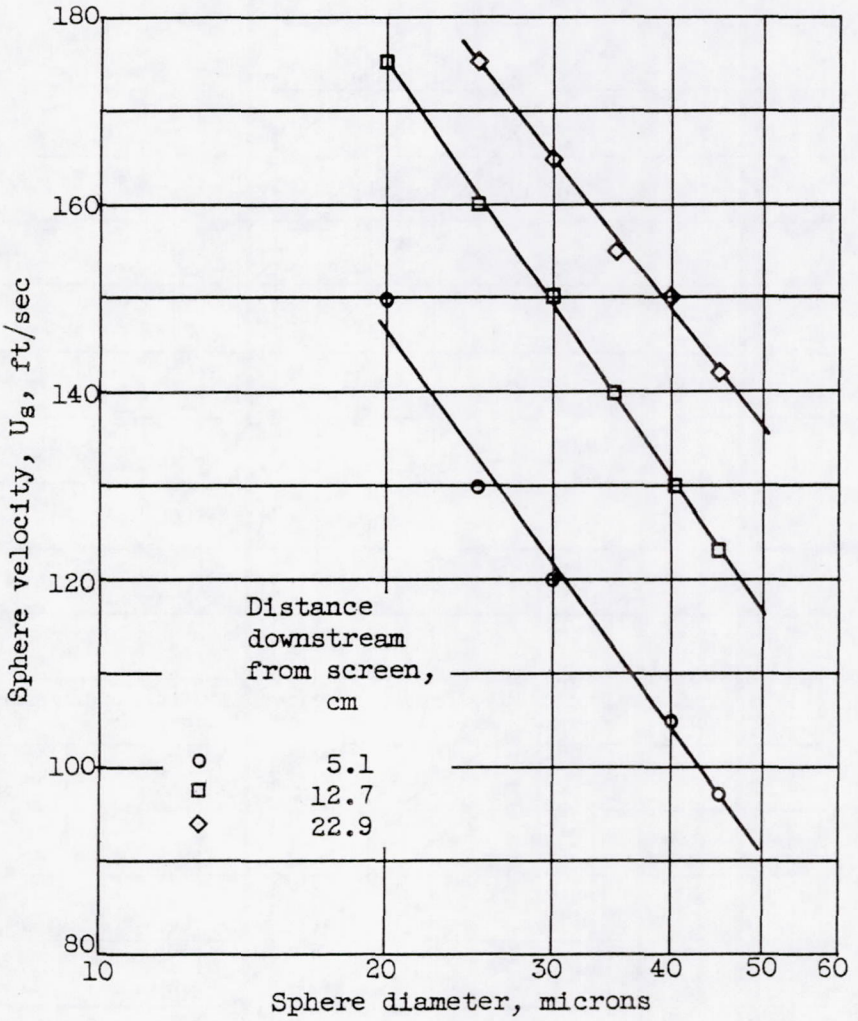

Figure 6. - Velocity and diameter data for magnesium spheres. Airstream velocity, 180 feet per second; air static pressure, 29.3 inches of mercury absolute; air temperature, 82° F.

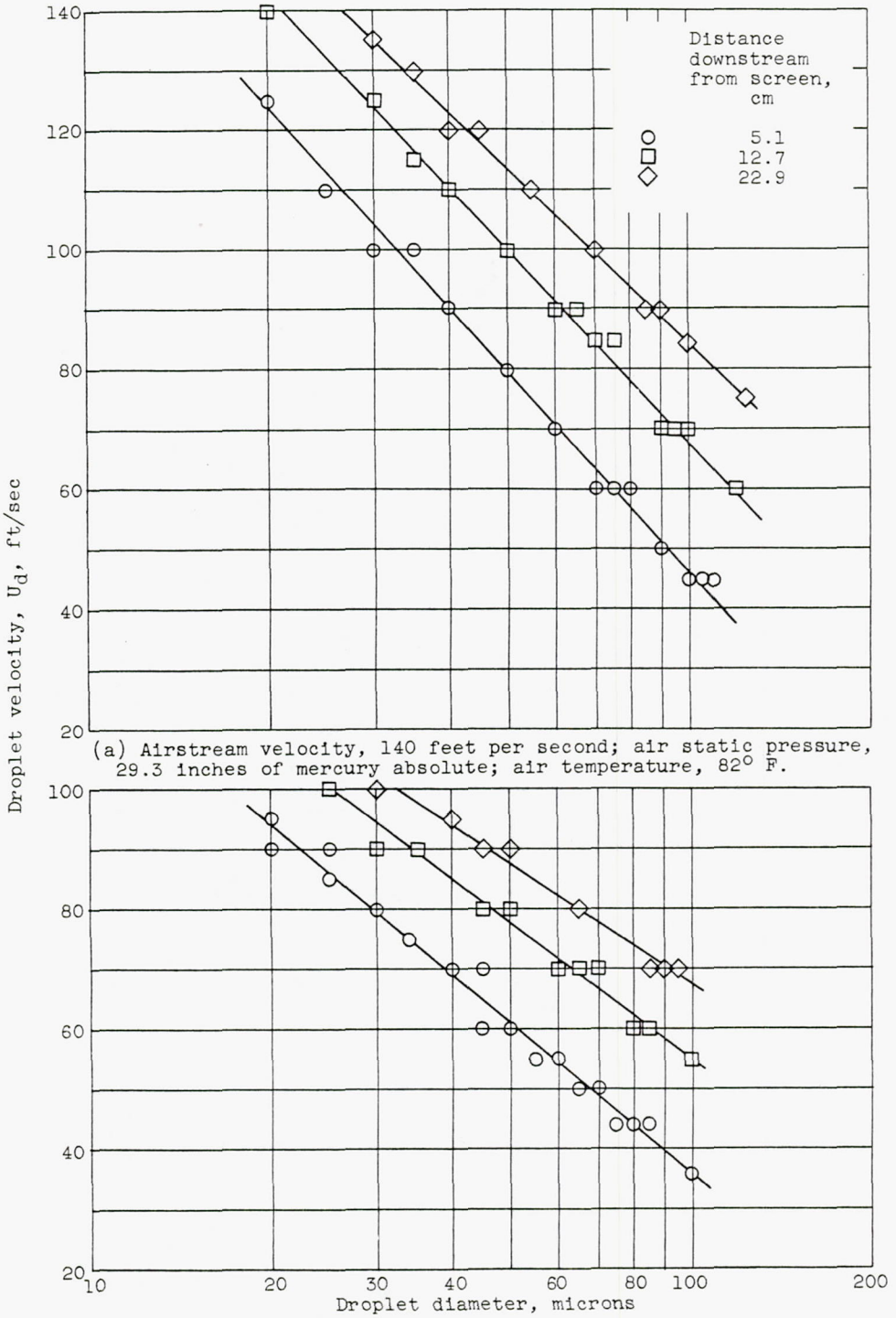

(a) Airstream velocity, 140 feet per second; air static pressure, 29.3 inches of mercury absolute; air temperature, 82° F.

(b) Airstream velocity, 100 feet per second; air static pressure, 41.2 inches of mercury absolute; air temperature, 82° F.

Figure 7. - Velocity and diameter data for trichloroethylene droplets.

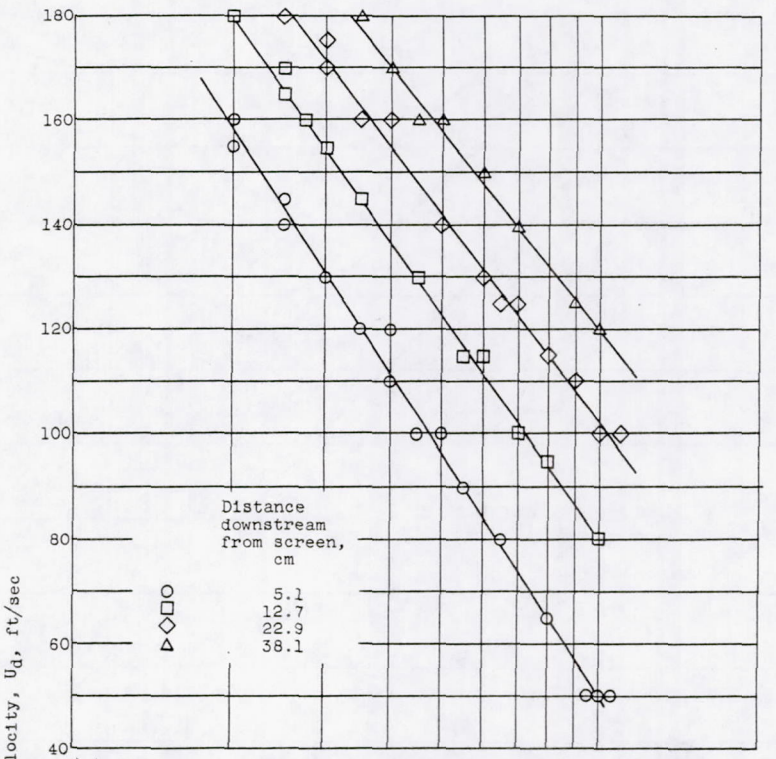

(c) Airstream velocity, 180 feet per second; air static pressure, 29.3 inches of mercury absolute; air temperature, 82° F.

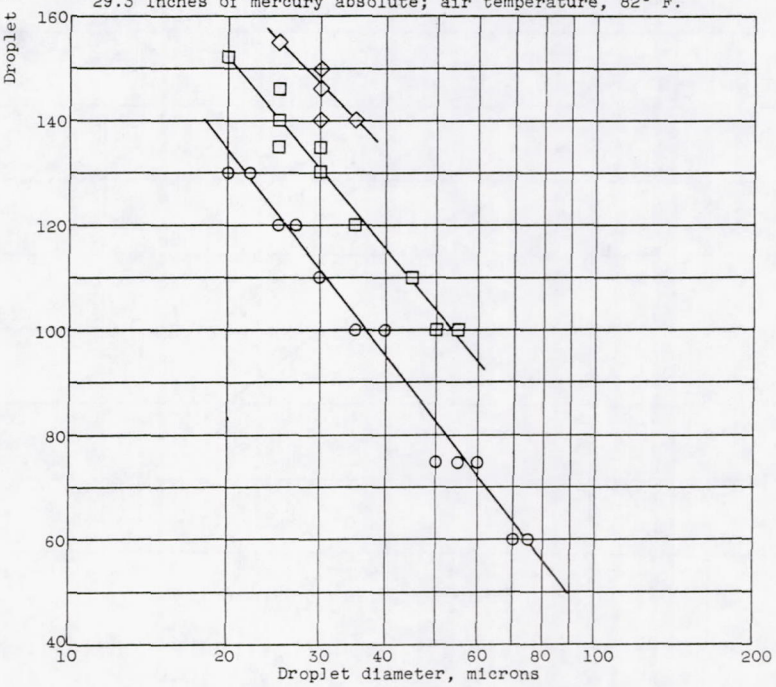

(d) Airstream velocity, 180 feet per second; air static pressure, 49 inches of mercury absolute; air temperature, 700° F.

Figure 7. - Concluded. Velocity and diameter data for trichloroethylene droplets.

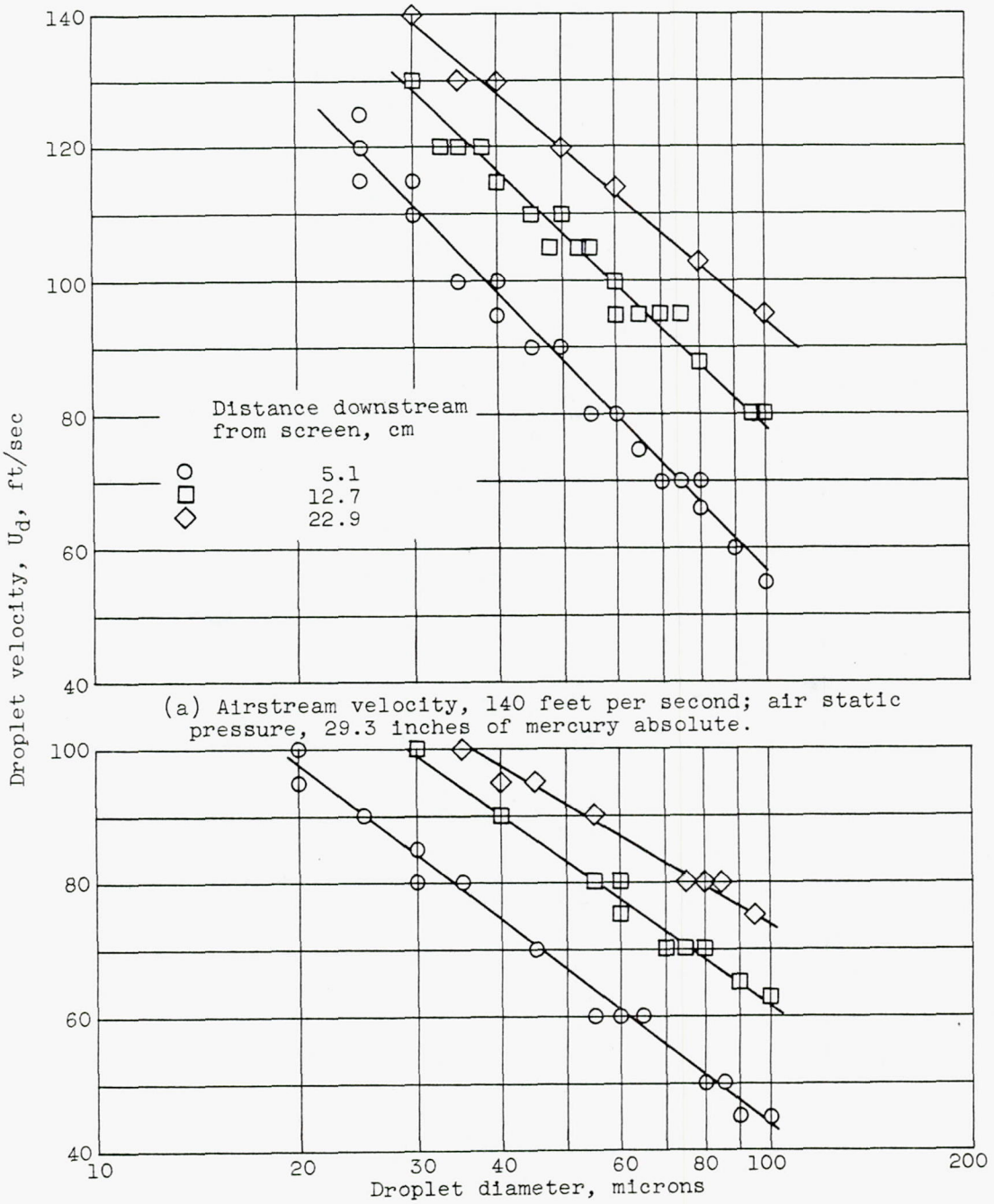

(a) Airstream velocity, 140 feet per second; air static pressure, 29.3 inches of mercury absolute.

(b) Airstream velocity, 100 feet per second; air static pressure, 41.2 inches of mercury absolute.

Figure 8. - Velocity and diameter data for water droplets. Air temperature, 82° F.

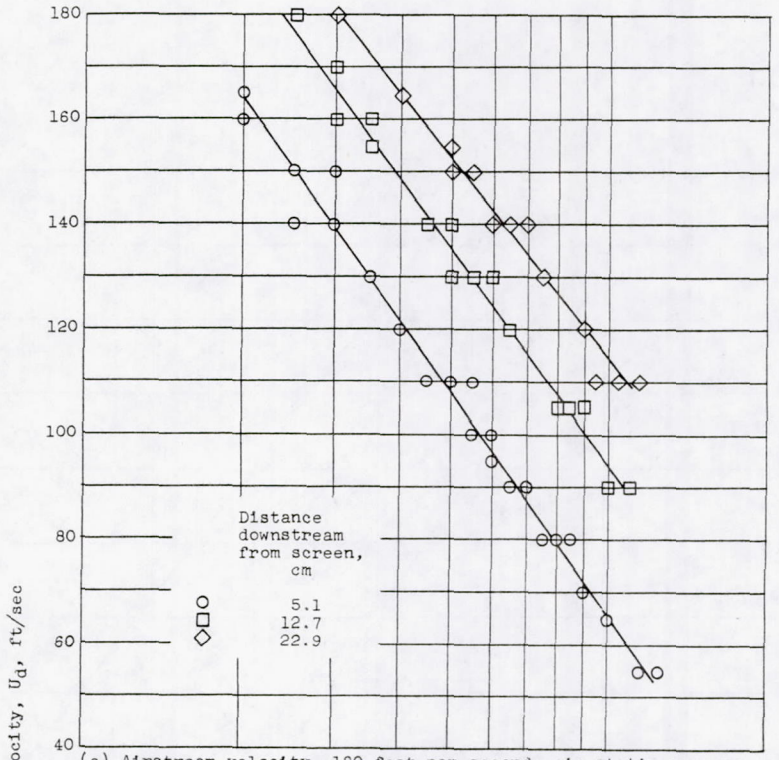

(c) Airstream velocity, 180 feet per second; air static pressure, 29.3 inches of mercury absolute.

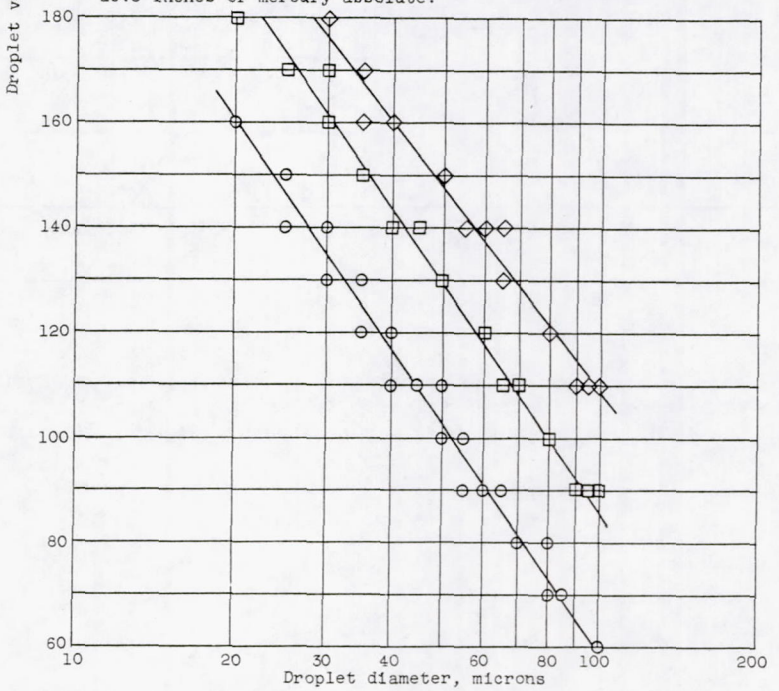

(d) Airstream velocity, 180 feet per second; air static pressure, 12.7 inches of mercury absolute.

Figure 8. - Concluded. Velocity and diameter data for water droplets. Air temperature, 82° F.

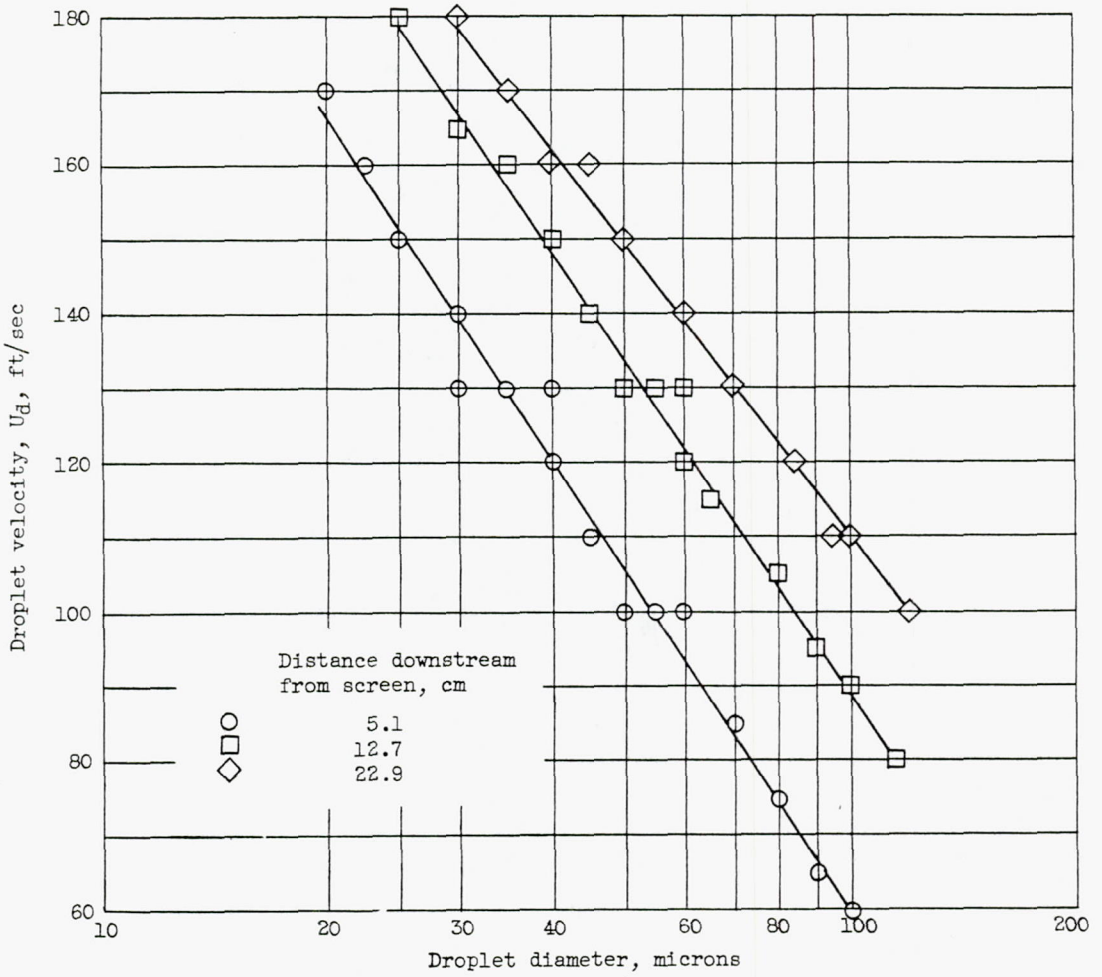

Figure 9. - Velocity and diameter data for water droplets for airstream saturated with water vapor. Airstream velocity, 180 feet per second; air static pressure, 12.7 inches of mercury absolute; air temperature, 40° F; wet-bulb temperature, 40° F.

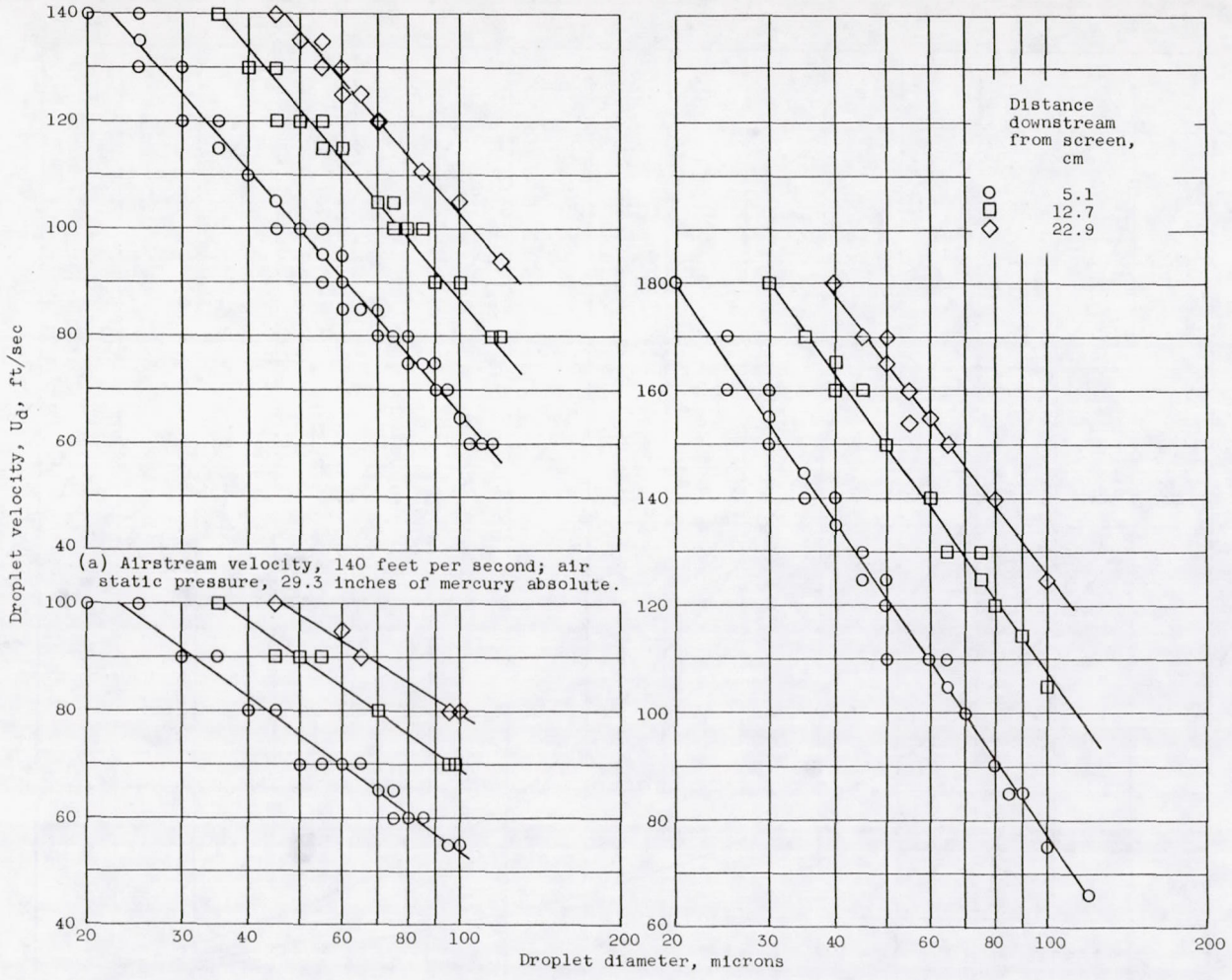

(a) Airstream velocity, 140 feet per second; air static pressure, 29.3 inches of mercury absolute.

(b) Airstream velocity, 100 feet per second; air static pressure, 41.2 inches of mercury absolute.

(c) Airstream velocity, 180 feet per second; air static pressure, 29.3 inches of mercury absolute.

Figure 10. - Velocity and diameter data for isooctane droplets. Air temperature, 82° F.

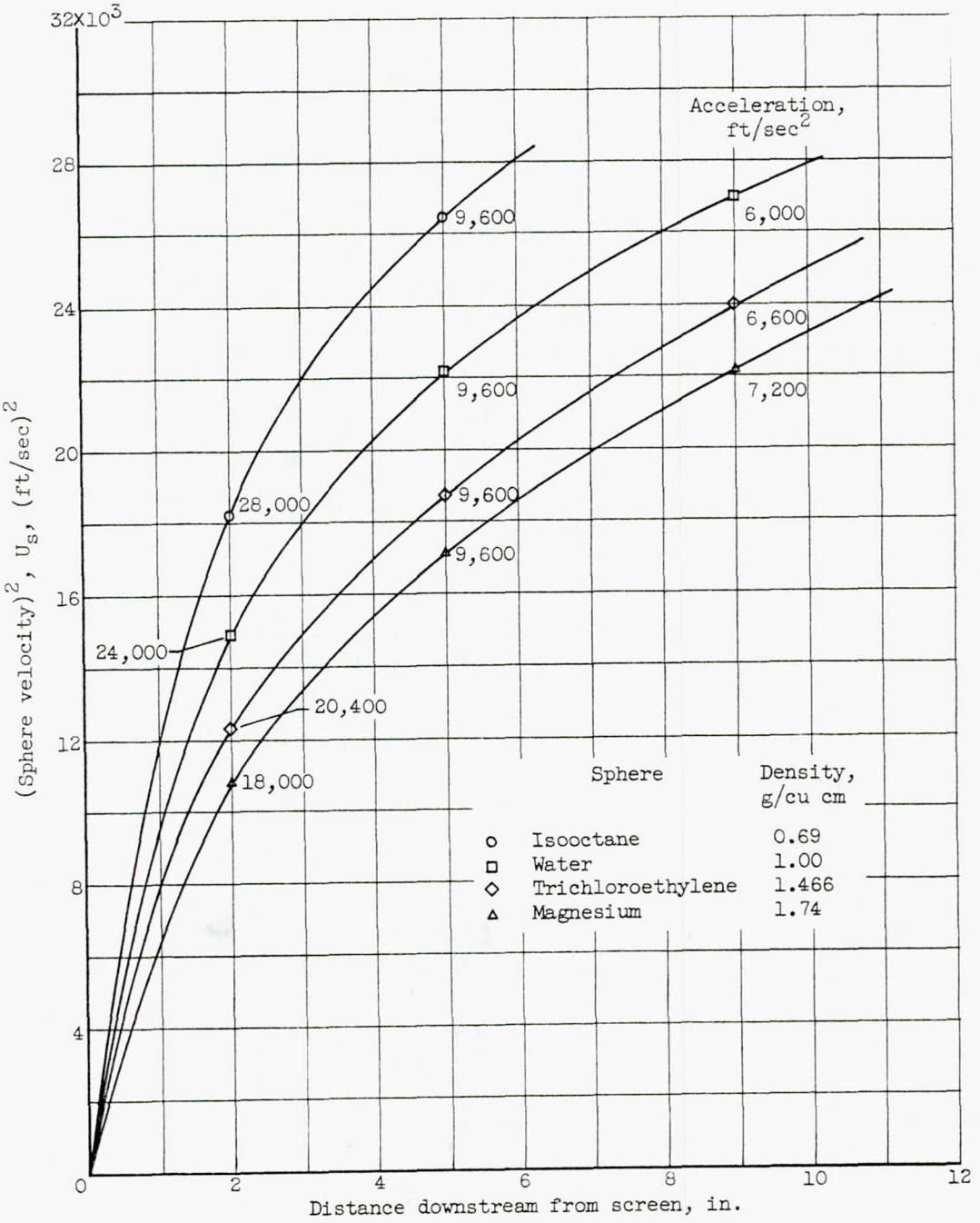

Figure 11. - Data plot for determining acceleration of liquid and solid spheres with initial diameters of 40 microns. Airstream velocity, 180 feet per second; air static pressure, 29.3 inches of mercury absolute; air temperature, 82° F.

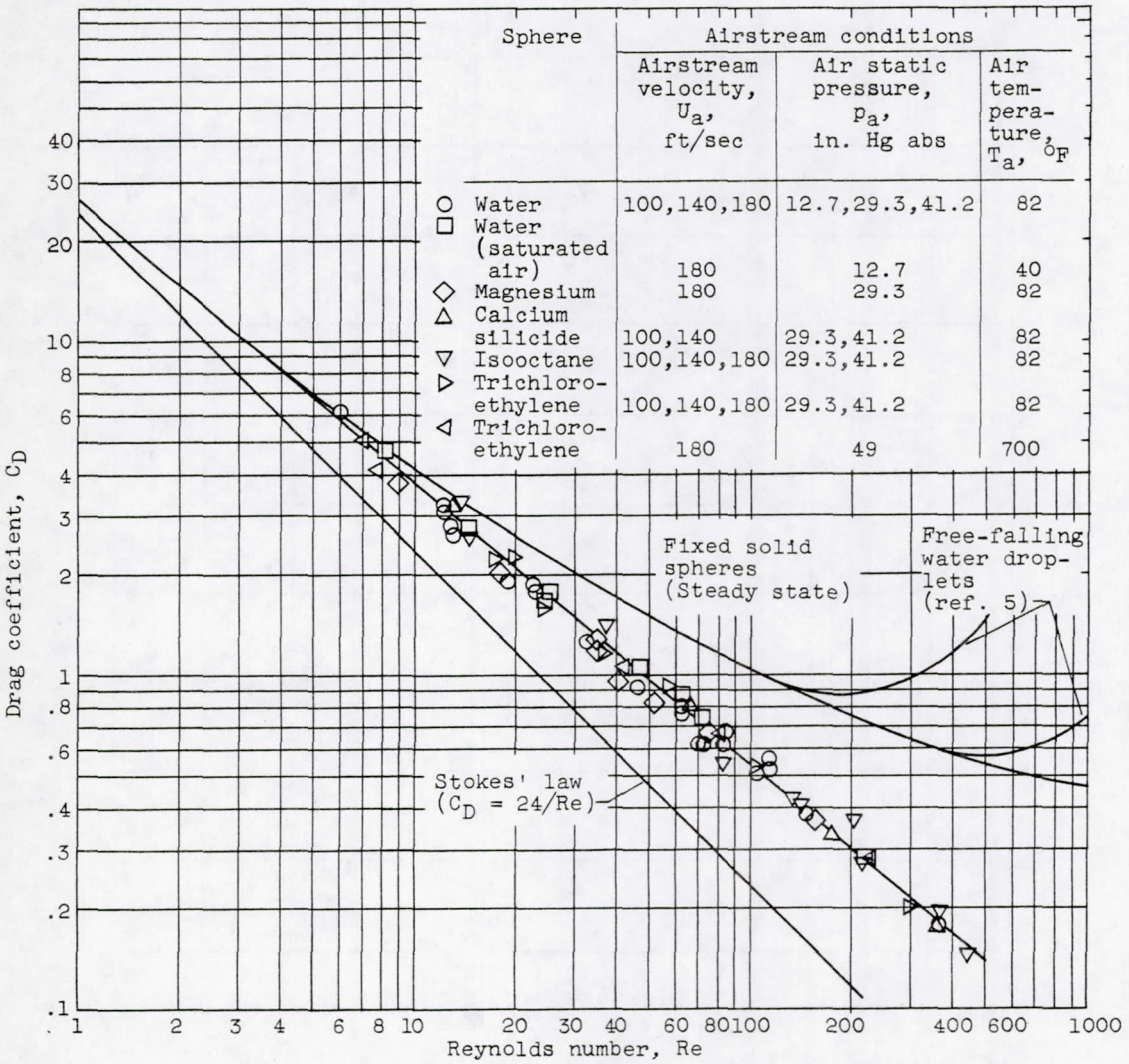

Figure 12. - Correlation of instantaneous unsteady-state drag coefficient (based on linear acceleration) with Reynolds number.

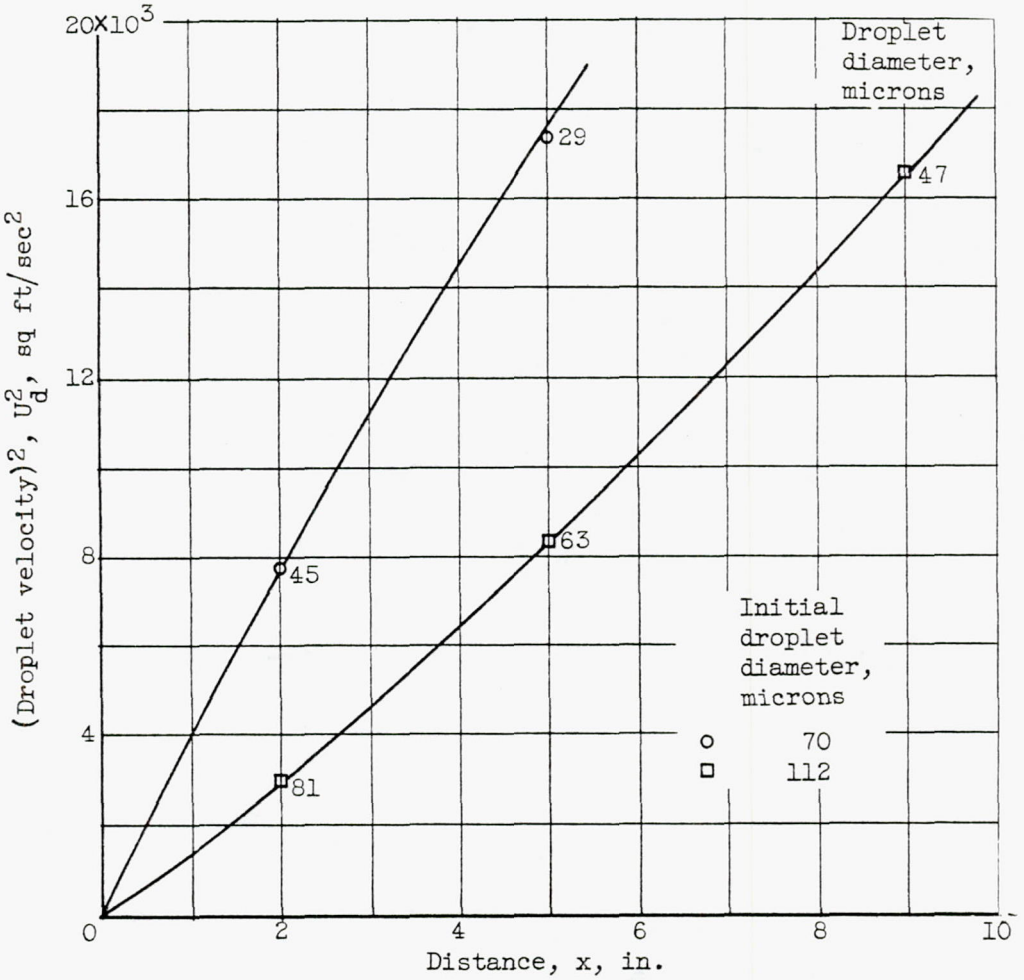

Figure 13. - Data plot for determining acceleration of trichloroethylene droplets. Airstream velocity, 180 feet per second; air static pressure, 49 inches of mercury absolute; air temperature, 700° F.

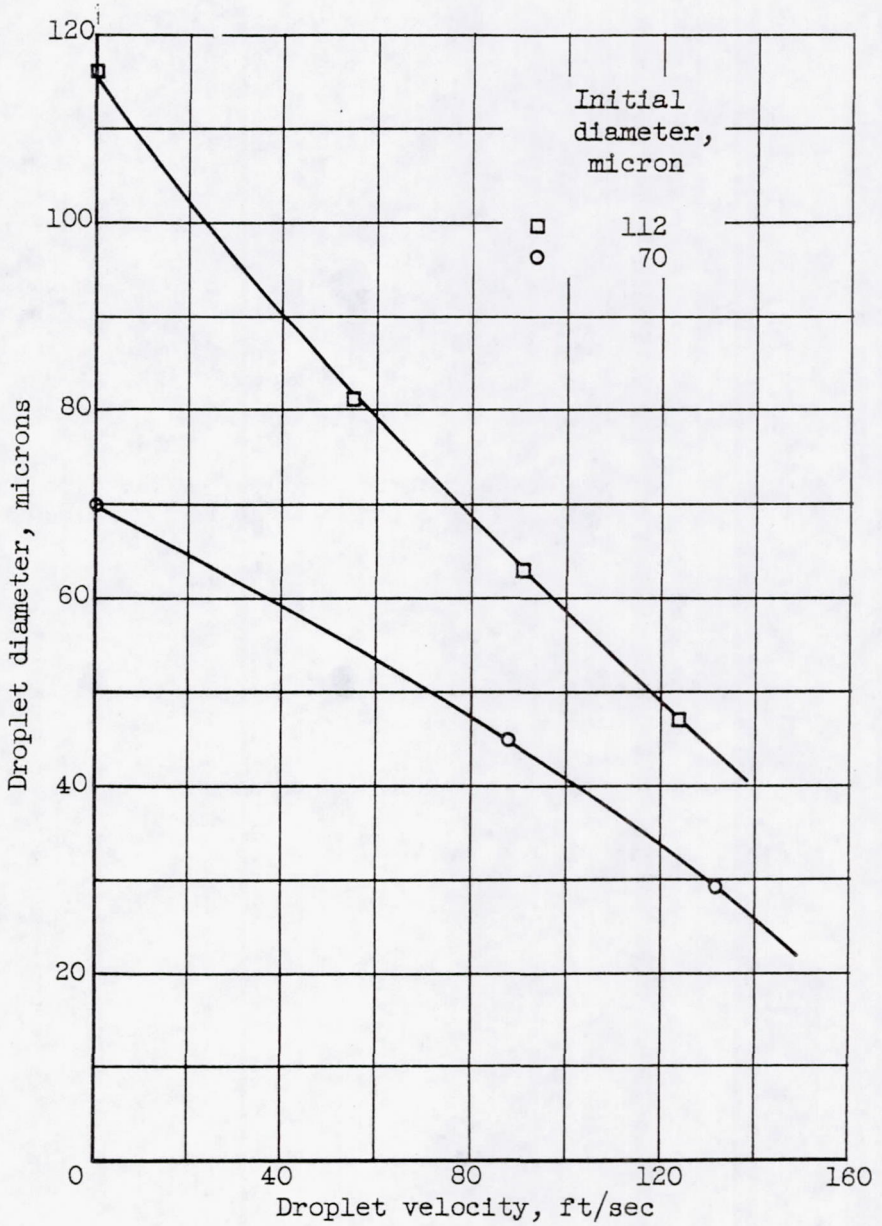

Figure 14. - Relation between droplet diameter and velocity for trichloroethylene. Airstream velocity, 180 feet per second; air static pressure, 49 inches of mercury absolute; air temperature, 700° F.